



Highly Ordered Mesoporous Hydroxide Thin Films through Self-Assembly of Size-Tailored Nano-Building Blocks: A Theoretical-Experimental Approach

メタデータ	言語: eng 出版者: 公開日: 2020-01-30 キーワード (Ja): キーワード (En): 作成者: Tarutani, Naoki, Tokudome, Yasuaki, Jobbágy, Matías, Soler-Illia, Galo J. A. A., Tang, Qiyun, Müller, Marcus, Takahashi, Masahide メールアドレス: 所属:
URL	http://hdl.handle.net/10466/00016710

Highly Ordered Mesoporous Hydroxide Thin Films through Self-Assembly of Size-Tailored Nano-Building Blocks: A Theoretical-Experimental Approach

Naoki Tarutani[†], Yasuaki Tokudome^{*†}, Matías Jobbágy[§], Galo J. A. A. Soler-Illia^{*#}, Qiyun Tang^{*‡}, Marcus Müller[‡], Masahide Takahashi[†].

[†]Department of Materials Science, Graduate School of Engineering, Osaka Prefecture University, Sakai, Osaka 599-8531, Japan

[§] INQUIMAE-CONICET, Facultad Ciencias Exactas y Naturales, Universidad de Buenos Aires, Buenos Aires, C1428EHA, Argentina

[#] Instituto de Nanosistemas, Universidad Nacional de General San Martín-CONICET, Av. 25 de Mayo y Francia, San Martín, 1650, Argentina

[‡] Institut für Theoretische Physik, Universität Göttingen, Friedrich-Hund-Platz 1, 37077 Göttingen, Germany

ABSTRACT: Mesoporous crystalline (hydr)oxides of low-valence metal ions (M(II) and M(III)) are highly demanded in the context of various applications. In this study, we demonstrate key factors to the successful formation of ordered mesoporous films through the Assembly of Nano-Building Block (ANBB) approach using a colloidal solution of crystalline $M(OH)_2$ ($M = Mn, Fe, Co, Ni,$ and Cu). The colloidal system of α -Ni(OH)₂ is presented in-depth as a typical example. Crystal growth and aggregation kinetics of the NBB were tuned by synthetic parameters. Nanometer-sized NBBs of tailored size between oligomer scale to over 20 nm were obtained. The films prepared from α -Ni(OH)₂ NBBs with a diameter of ≤ 7.5 nm showed ordered mesostructures through evaporation-induced self-assembly in the presence of supramolecular templates. Coarse-grained simulation suggests that there is a threshold diameter of NBB toward the formation of well-ordered mesostructures. It was found that, as well as limiting the diameter of NBB, inhibition of an aggregation of NBBs by using coordinative additives or diluting the NBB colloidal solution were essential to control the assembly of NBBs and templates into the ordered mesostructures. The results obtained here open up the synthesis of ordered mesoporous materials with a crystalline wall of variety of chemical compositions containing low-valence metal elements.

Introduction

The bottom-up synthesis of mesoscale architectures from pre-formed nano-building blocks (NBBs) is a promising way to design materials with complex architectures with position-defined functions. In the last few years, superstructures constituted of nanocrystals,¹ anisotropic oriented structures,² porous systems,³ gradient periodic structures⁴ and co-continuous structures⁵ fabricated through the NBB approach have been reported. These architectures show advantageous characteristics in wide application fields such as catalysts,⁶ optical materials,⁷ and energy storage.⁸ The chemical composition and the crystalline phase of these materials can be tuned by tailoring the respective NBBs. Moreover, specific interfaces and heterostructures can be formed by the use of NBBs with different chemical and structural features. Intrinsic properties of NBBs are then combined, and a synergic effect leads to novel functionalities.^{9,10}

In the case of ordered mesoporous materials, a key limitation of the conventional methods that use molecular metal precursors is dealing with the complex dynamics of their chemical reactivity in solution, and their self-assembly with the templates. The variety of chemical behaviors is such that a general route to materials with precise tuning of the porosity, composition and wall crystallinity is **still difficult to establish**. This limitation is expected to be overcome by using pre-

programmed NBBs precursors, which can be tailored in order to attain crystalline walls composed of arbitrarily desired chemical compositions and crystallite size, as well as pre-programmed interactions with the template.

The desired architectural features of mesostructured and mesoporous materials are regulated by the NBB diameter, (D_{NBB}) and the interactions between the organic and inorganic NBBs.¹¹ Assembly of NBBs (ANBB) approach has been employed for the fabrication of ordered mesoporous materials with enhanced liquid/ion diffusion, high specific surface area, and alignment of the pores. However, the preparation of single-nm-sized “crystalline” NBBs and their assembly into ordered mesostructures are so far limited to high-valence metal oxides such as ZrO₂, TiO₂, and CeO₂.¹²⁻¹⁴ Technologically valuable crystalline (hydr)oxides of low-valence metal elements (M(II) and M(III)) rapidly form coarse μ m-sized crystals and aggregates, which prevents assembly into ordered mesostructures. These materials are highly desirable in electrochemical catalysts, sustainable energy devices, and environmental treatment.¹⁵⁻¹⁸

Recently, we reported the preparation of single-nm-sized low-valence metal hydroxide nanocrystals with a variety of chemical compositions.¹⁹ The nanocrystals were obtained as colloidal solutions, which were used as inorganic NBBs to form mesoporous structures via an evaporation-induced self-

assembly (EISA) process. While this breakthrough permitted to access several (hydr)oxide frameworks, the effect of diameter and stability of the metal hydroxide NBBs, which in turn depends on a chemical composition of NBBs, on the final mesoporous structures are only incompletely understood despite of their significance. Although the size of the inorganic cluster, and their interactions with templates have been demonstrated to be fundamental parameters for the successful formation of mesostructures in amorphous silica systems,^{20,21} there are no versatile and quantitative insights which are widely applicable to crystalline NBBs with various chemical compositions. As a result, the formation of ordered mesoporous structures is still limited to NBBs of particular compositions. Our motivation in the present work is to develop a versatile ANBB principal to access to the greatest variety of crystalline mesoporous materials based on a comprehensive experimental study combined with simulation tools that permit to gain a quantitative insight in the fundamental role of NBB size and interactions in mesostructure formation.

Herein, we demonstrate key factors towards the compositionally versatile formation of crystalline ordered mesoporous films from metal hydroxide NBBs through an integrated theoretical-experimental approach. The diameter and the aggregative tendency (surface nature) of NBBs were tuned by synthetic parameters of the epoxide-mediated alkalization process, and their effects on the final mesoporous structures were systematically investigated. We successfully controlled the D_{NBB} from the oligomeric scale to over 20 nm by tuning the amount of additives and reaction time. Ordered mesoporous films were found to form through an EISA process for D_{NBB} smaller than a threshold value. Simulation studies showed a good agreement with experimental, indicating that there is a threshold of D_{NBB} toward the formation of well-ordered mesostructures. It was found that the aggregation tendency of NBBs is another important factor for the formation of well-defined mesostructures. The crystallization and aggregation of NBBs strongly depend on the chemical composition of the starting solutions. The present tunable synthesis route of NBBs with a variety of compositions gives us general insights about NBBs for the successful formation of ordered mesostructures (hydroxide of Mn, Fe, Co, Ni, and Cu). Moreover, the mesoporous metal hydroxide films produced through this route can be transformed into oxides, sulfide, and carbon/metal composites by an adequate design of the NBB precursor and post-treatment. The present synthesis is therefore promising to improve the functional properties of diverse mesoporous materials.

Experimental

Chemicals.

Manganese(II) chloride tetrahydrate ($\text{MnCl}_2 \cdot 4\text{H}_2\text{O}$, 99.0%), iron(II) chloride tetrahydrate ($\text{FeCl}_2 \cdot 4\text{H}_2\text{O}$, 99.0–102.0%), cobalt chloride hexahydrate ($\text{CoCl}_2 \cdot 6\text{H}_2\text{O}$, 99.0%), nickel chloride hexahydrate ($\text{NiCl}_2 \cdot 6\text{H}_2\text{O}$, 98.0%), copper chloride dihydrate ($\text{CuCl}_2 \cdot 2\text{H}_2\text{O}$, 99.0%) acetic acid (99.7%), acrylic acid (99%), glutaric acid (98.0%), citric acid (98.0%), ethanol (99.5%), (\pm) propylene oxide (> 99%), and Pluronic F127 (poly(ethylene oxide)-poly(propylene oxide)-poly(ethylene oxide), PEO-PPO-PEO) were used as received. Acrylic acid, propylene oxide and F127 were purchased from Sigma-Aldrich Co. All other reagents were purchased from Wako Pure Chemicals Industries, Ltd. Ultrapure water of 18.2 $\text{M}\Omega\cdot\text{cm}$ resistivity was used in all experiments.

Synthesis of $\alpha\text{-Ni}(\text{OH})_2$ NBBs.

$\text{NiCl}_2 \cdot 6\text{H}_2\text{O}$ (0.5 mmol) and a given amount of carboxylic acid (acrylic acid or acetic acid) (molar ratio of carboxylic acid to nickel chloride was 0–4.0) were dissolved in an ethanol (1.0 mL) at 25 °C. Propylene oxide (7.5 mmol) was added to the clear precursor solution and stirred for 30 s. Resultant homogenous solutions were left at room temperature (20–25 °C). Variety of in-situ measurements were taken during reaction progress. After an appropriate time, the samples were dried at 60 °C for 20 h. The sample IDs prepared through this process are denoted as $x\text{-}y\text{-}t$, where x is the type of acid (AA; acrylic acid and AcOH; acetic acid), y is the molar ratio of carboxylic acid to nickel chloride, and t is the time (min) since the addition of propylene oxide.

Synthesis of mesoporous $\alpha\text{-Ni}(\text{OH})_2$ cast-films.

$\text{NiCl}_2 \cdot 6\text{H}_2\text{O}$ (0.5 mmol), carboxylic acid (acrylic acid or acetic acid) (0–4.0 mmol) and template surfactant (F127) (2.5 μmol , $[\text{F127}]/[\text{Ni}^{2+}] = 0.005$) were dissolved in ethanol (1.0 mL) at 20–25 °C. After the addition of propylene oxide (7.5 mmol), the solution was stirred for 30 s and left at 20–25 °C. The reacting solution was casted on glass (76 mm \times 26 mm) or Si substrates (\sim 20 mm square) after an appropriate time and allowed to evaporate under ambient conditions (temperature; 20–25 °C, humidity; 50–70 %) for 2 h. As-synthesized films were left in an oven at 60 °C for 2 h, followed by a treatment at 120 °C for 2 h. To remove polymer templates, films were heat treated at 250 °C for 2 h. The sample IDs are denoted as F- $x\text{-}y\text{-}t$, where x , y , and t are same as described above.

Synthesis of mesoporous $\text{M}(\text{OH})_2$ ($\text{M} = \text{Mn}(\text{II}), \text{Fe}(\text{II}), \text{Co}(\text{II}), \text{Ni}(\text{II})$ and $\text{Cu}(\text{II})$) cast-films.

$\text{MCl}_2 \cdot n\text{H}_2\text{O}$ ($\text{M} = \text{Mn}(\text{II}), \text{Fe}(\text{II}), \text{Co}(\text{II}), \text{Ni}(\text{II})$ and $\text{Cu}(\text{II}), n = 2\text{--}6$) (0.5 mmol), carboxylic acid (acrylic acid (4.0 mmol), glutaric acid (1.0 mmol), or citric acid (0.67 mmol)) and F127 (2.5 μmol) were dissolved in an ethanol (1.0 mL) at 20–25 °C. After the addition of propylene oxide (7.5 mmol), the solution was stirred for 30 s and left at 20–25 °C. The reacting solution was casted on glass substrate after an appropriate time, and then allowed to evaporate under an ambient condition (temperature; 20–25 °C, humidity; 50–70 %) for 2 h. The sample IDs are denoted as M- $x\text{-}y\text{-}t$, where M is metal ion (Mn, Fe, Co, Ni and Cu), x is kind of carboxylic acid (AA: acrylic acid, Glu: glutaric acid, and Cit: citric acid), y and t are same as described above, respectively.

Simulation studies.

A coarse-grained model of $\alpha\text{-Ni}(\text{OH})_2$ NBBs and amphiphilic surfactant, F127, was employed to study the formation of mesostructures. The $\alpha\text{-Ni}(\text{OH})_2$ NBBs were represented by spherical nanoparticles with variable diameters, and the surfactant F127 was described by a soft bead-spring model of a BAB triblock copolymer (PEO-PPO-PEO). The effect of solvents such as water and acid are taken into account in the interactions between NBBs and surfactants.²² The Hamaker potential was chosen for NBB-NBB interaction, in which the magnitude of the potential depends on the D_{NBB} . Details of the model are summarized in the SI.

The dispersity index (DI) was calculated to evaluate the homogeneity of mesostructures. The DI is defined as $\text{DI} = S_w/S_n$, where $S_w = \sum_i n_i \sigma_i^2 / \sum_i n_i \sigma_i$ is the weight average pore area and $S_n = \sum_i n_i \sigma_i / \sum_i n_i$ is the number average pore area. Here n_i is the number of mesopores with area, σ_i , obtained from 10 independent simulations; in each simulation 100 configurations are selected for the DI calculation.

Characterization.

A transmission electron microscope (TEM; JEM-2000FX, JEOL, Japan) and scanning TEM (STEM; JEM-2100F, JEOL, Japan) were employed at an operating voltage of 200 kV to observe primary particles and mesostructures of the samples. Powder X-ray diffraction (PXRD) (Multiflex, Rigaku, Japan) using Cu K α radiation ($\lambda = 0.1544$ nm) was used to characterize crystal phases of dried powdery samples. Fourier transform infrared (FT-IR) spectroscopy (ALPHA FT-IR spectrometer, Bruker Optik GmbH, Germany) and ultraviolet-visible-near infrared (UV-Vis-NIR) spectroscopy (V-670 spectrophotometer, JASCO Corp.) were used to analyze chemical bonding and coordination state of Ni(II). Conductivity and pH of solutions were collected using a water quality meter (D74, Horiba, Japan) with respective glass electrodes (3552-10D and 9618-10D). Thermogravimetric-differential thermal analysis (TG-DTA; Thermo plus Evo, Rigaku, Japan) was carried out at a ramp rate of 10 °C/min while continuously supplying atmospheric air at a rate of 0.3 L/min. The mesoporous characteristics of samples heat-treated at 250 °C were analyzed by N₂ sorption measurements (Belsorp-mini II, Bel Japan Inc., Japan). Small angle X-ray scattering (SAXS) measurement was performed to characterize the D_{NBB} and mesostructures with the beamline of the Brazilian Synchrotron Light Laboratory (LNLS, Brazil D11A-SAXS1-18927 and 20160366). A polyimide film was used to pack and measure the powder samples. The D_{NBB} is defined as the diameter of aggregates when primary particles form aggregation. Details of characterization are described in the SI.

Results and discussion

Synthesis of α -Ni(OH)₂ NBBs of controlled diameter.

Uniform colloidal dispersions of nickel hydroxides with particle diameters ranging from 2 to 20 nm were obtained after aging the metal chloride in the presence of propylene oxide and an organic acid at room temperature. Hydrolysis of propylene oxide increases the solution pH homogeneously,²³ inducing a high degree of supersaturation to form nm-sized hydroxide crystals,²⁴ while the organic acid controls the growth kinetics of the metal hydroxide. Figure 1a shows a typical colloid sample obtained from the reaction mixture containing NiCl₂·6H₂O and acrylic acid (AA-2.0-60). The powder obtained by drying the colloidal dispersion can be identified as nanometer sized α -Ni(OH)₂ which grow preferentially along the *c* axis (Figure 1b). The absence of a 110 peak in the nanocolloid samples indicates both the formation of small crystals along the 110 direction (consistent with the isotropic particles observed by TEM, see below), as well as the introduction of defects, including the formation of a turbostratic ordering, which is a well-known feature of α -Ni(OH)₂ 110 planes.^{25,26} Acrylic acid was mandatory to yield a stable colloidal solution. Indeed, opaque gelatinous products due to high aggregation of the inorganic building blocks were obtained from a reaction mixture without acrylic acid (Figure S1). This result suggests that the addition of acrylic acid is a key factor to control the crystal growth and to inhibit the aggregation of nanocrystals.

One desirable feature of this synthetic pathway is the possibility of an accurate kinetic and thermodynamic control of D_{NBB} through external synthetic variables such as initial concentrations, amount of propylene oxide, type of acid employed, or reaction time.

This approach is illustrated by analyzing in-depth a reactive system that uses acrylic acid as a growth controller.

Figure 2a shows the evolution of D_{NBB} as a function of the reaction time for an exemplary system, AA-2.0-*t* systems, which evolves for *t* = 1–60 min. D_{NBB} were estimated from the in-situ SAXS patterns collected for the reacting medium (see experimental in SI and Figure S2 for the details). A linear increase of the D_{NBB} is observed, from the oligomer scale to ~ 1.5 nm in the first 15 minutes. The growth levels off in a second step, and the final diameter is almost reached in the first 30 min, which is in a good agreement with the time scale of the consumption of ionic species. The relative amount of Ni(II) ion decreases to 6.1% of the initial concentration within 30 min reaction. The crystal growth of layered nickel hydroxide was reported to take place through rapid edge-on condensation of partially hydrolyzed Ni species, followed by a relatively slow stacking of the sheets.²⁴ In the present case, the extended growth of the constituent sheets was successfully retarded by the addition of acrylic acid. FT-IR, UV-Vis-NIR, and PXRD measurements revealed that most changes due to nanocrystal growth take place in the first 30 minutes of reaction (Figure S3). Racah B parameter and crystal field energy of AA-2.0-*t* were estimated from UV-Vis-NIR spectra and reached constant values comparable with reported α -Ni(OH)₂ (Figure S3b and S3d),^{27,28} which means brucite-like hydroxide sheets were successfully formed. FT-IR signals belonging to the asymmetric $\nu(\text{COO})_{\text{as}}$ and symmetric $\nu(\text{COO})_{\text{s}}$ acrylate vibrations were observed in the 1582–1552 cm⁻¹, and 1428 cm⁻¹ regions, respectively (Figure S3a). The frequency differences $\Delta = \nu(\text{COO})_{\text{as}} - \nu(\text{COO})_{\text{s}}$, were in the range of 124–154 cm⁻¹, which is relatively larger or comparable to that of free acrylate ($\Delta = 110$ –140 cm⁻¹).²⁹ These results suggest acrylate ion is unidentately coordinated to Ni(II) and intercalated/adsorbed on α -Ni(OH)₂ sheets.²⁸ It can be concluded that acrylic acid is present in the NBB through unidentate coordination to a small number of Ni(II) centers, and intercalation.

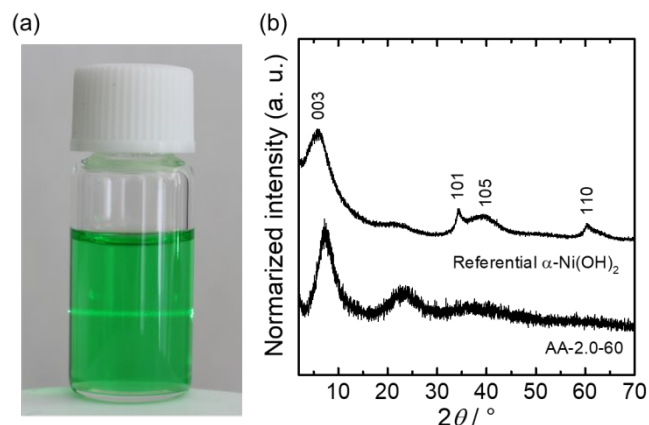


Figure 1. (a) Transparent solution of AA-2.0-60 showing Tyndall effect. (b) PXRD pattern of powder collected by drying AA-2.0-60 solution. The referential pattern was acrylate intercalated α -Ni(OH)₂ prepared by a standard precipitation method (see experimental section in SI).

Individual nanocrystals remain well dispersed in the initial solutions when AA/Ni > 2.0. The STEM image of synthesized NBB (Figure 2b) shows that the D_{NBB} was 1.7 nm without aggregation, which supports the result of SAXS measurement. The shoulder of SAXS curves gradually shifted to lower scattering vector with increasing the intensity (Figure S4). The diameter of NBB obtained under these synthetic conditions is relatively small compared to previously reported oxide systems (~ 5 nm),¹²⁻¹⁴ which should allow the flexible

tuning of the mesostructure through controlled interactions among organic and inorganic NBBs.

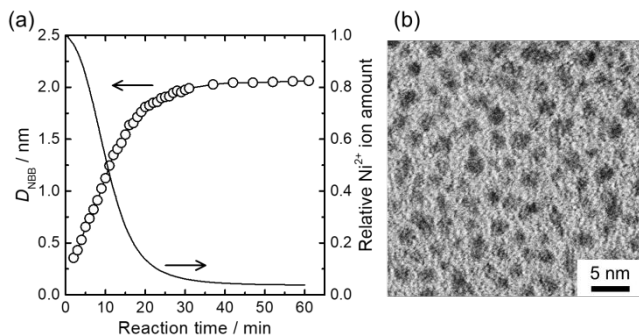


Figure 2 Time evolution of D_{NBB} (open circle) and consumption of ionic Ni species (solid line) (calculated from conductivity of solution, see supporting information, SI) in the reacting solution of AA-2.0- t ($t = 1-60$ min). (b) STEM image of AA-2.0-60 dried on a TEM copper grid.

TEM observations indicated that samples obtained from solutions with lower amount of acrylic acid (AA/Ni < 2.0) were composed of aggregated fine nanoparticles (experimental section supporting information, Figure S4). Therefore, a hierarchically structured model was employed for fitting the SAXS curves of reactive systems containing lower amount of organic acids, i.e., AA- y - t ($y = 0-1.0$, $t = 1-60$ min), in order to take into account the aggregation of the NBBs. Time-evolution of primary and secondary particle diameters are presented in Figure 3a. All solutions contained secondary particles after an appropriate reaction time. The nanoparticle growth rates were estimated by linear fitting of the obtained plot. The primary particles grew at a rate of 0.37 nm/min (AA-0- t), 0.25 nm/min (AA-0.1- t), 0.33 nm/min (AA-0.5- t) within the first 10 min, and the diameter of the primary particles, D_p , reached a value of ~2.0 nm irrespective of the amount of acrylic acid. On the other hand, the growth rates of the secondary particles, D_s , were retarded by increasing amounts of acrylic acid (AA-0- t ; 7.5 nm/min, AA-0.1- t ; 2.9 nm/min, AA-0.5- t ; 0.61 nm/min). Figure 3b shows D_{NBB} prepared with various amounts of acrylic acid after 30 min reaction (D_p or D_s were used as D_{NBB} for the system without or with aggregation, respectively). It is clearly observed that D_{NBB} decreased from > 20 nm (aggregated particles) to ~2 nm (isolated particles) with increasing amounts of acrylic acid. The acrylic acid/acrylate incorporated in the solid phase increases along with the nominal molar AA:Ni ratio, and saturates at a value of 1.5 AA species for Ni ion at a nominal AA:Ni value of 2 (Figure S5). These results indicate that acrylic acid not only retards the crystallization but also suppresses the aggregative tendency of NBBs, through coordination, intercalation, and surface modification.

In summary, D_{NBB} were successfully controlled from oligomer scale to > 20 nm by tuning the reaction time and the amount of acrylic acid. This procedure permits to tailor the size and interactions between the inorganic NBBs, in order to create hybrid meso-architectures. It is important to stress that after reaction completion (i.e., removal of Ni(II) from solution), no significant changes are observed in D_{NBB} for several days, so it can be reasonably concluded that after a first kinetic evolution, the control of D_{NBB} is attainable in a practically thermodynamic fashion.

The effect of D_{NBB} on the formation of mesoporous structures

The α -Ni(OH)₂ NBBs could be produced with tuned diameters, and were used to elucidate dominant factors towards the successful formation of mesoporous crystalline films. A nonionic block-copolymer, F127, was used as the supramolecular pore template. The addition of F127 to the initial solutions had little effect on the growth and aggregation of NBBs (Figure S6). Thanks to that, the controlled drying of cast sols containing the template allowed for the co-self-assembly of NBBs and F127 templates.

Solutions containing NBBs of varying D_{NBB} from 0.74 to 26 nm were employed to fabricate mesostructured films through the EISA process, in a systematic experiment (Figure 4a). The cast-film prepared by using NBBs of $D_{\text{NBB}} \leq 7.5$ nm showed SAXS peaks assigned to an organized mesostructure. According to SAXS pattern indexing (Figure 4a) and TEM micrographs (Figure 4b) in which 110 pore planes are evident, it was possible to identify these organized samples as an Im(-3)m cubic-like pore pattern formed by inorganic NBB located around initially spherical micelles. This information is consistent with the mesophases previously reported; the used metal:template ratio ($[\text{F127}]/[\text{Ni}^{2+}] = 0.005$) is similar to those usually employed in the literature for obtaining a body-centered cubic mesostructure in silica and titania.^{30,31} The obtained ordered 3D cubic mesostructure was maintained even after removal of F127 template by heat treatment at 250 °C. The corresponding N₂ adsorption-desorption isotherms (Figure S7) obtained on films heat treated at 120 °C for 2 h and 250 °C for 2 h can be classified into a type IV shape with a hysteresis loop classified as an intermediate between H1 and H2 (i.e., smooth adsorption and almost parallel adsorption and desorption branches) which is typical of pores with constrictions.³² Pore diameter, wall thickness, specific surface area, and pore volume for a typical sample (AA-2.0-F-5) are 7.6 nm, 6.5 nm, 79.2 m²/g, and 0.140 cm³/g, respectively.

The samples prepared with NBB of $4.7 \text{ nm} \leq D_{\text{NBB}} \leq 7.5 \text{ nm}$ showed a broad peak at $q \sim 0.5 \text{ nm}^{-1}$. The broadening of the peak for these samples reveals that the mesostructure becomes less-ordered when larger inorganic NBB are used as precursors.

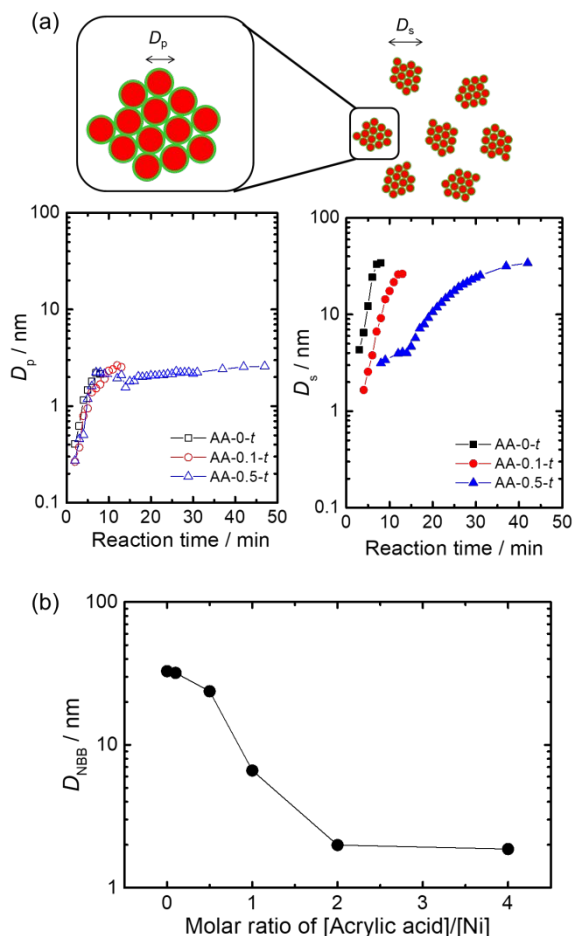


Figure 3. (a) Time-dependent growth of the diameters of primary particles, D_p (open symbols), and secondary particles, D_s (close symbols), prepared from AA-0- t (black), AA-0.1- t (red), and AA-0.5- t (blue) ($t = 1-60$). (b) Molar ratio ([AA]/[Ni]) dependence of D_{NBB} (D_s when AA/Ni ≤ 1.0 and D_p when AA/Ni ≥ 2.0) of AA- y -30 ($y = 0-4.0$).

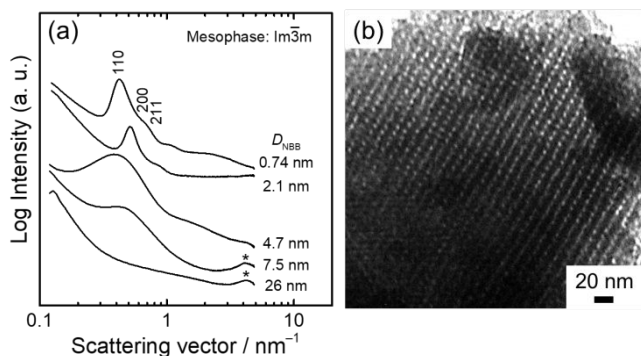


Figure 4. (a) SAXS patterns of cast-films after drying at 120 °C for 2 h. The casted-films composed of $D_{\text{NBB}} = 0.74$ nm, 2.1 nm, 4.7 nm, 7.5 nm, and 26 nm were prepared from F-AA-2.0-5, F-AA-2.0-60, F-AA-0.5-15, F-AA-1.0-45, and F-AA-0.1-15, respectively. *: background peaks from α -Ni(OH)₂ and polyimide. (b) TEM image of films prepared from AA-2.0-F-5 after heat treatment at 120 °C for 2 h and 250 °C for 2 h.

The samples prepared with NBB of $4.7 \text{ nm} \leq D_{\text{NBB}} \leq 7.5 \text{ nm}$ showed a broad peak at $q \sim 0.5 \text{ nm}^{-1}$. The broadening of the peak for these samples reveals that the mesostructure becomes less-ordered when larger inorganic NBB are used as precursors.

In order to understand the role of the NBB size on the formation of organized mesostructures, we performed a simulation study that takes into account the size and interactions of the inorganic NBB and the templates. The model considers n amphiphilic surfactants and n_p nanoparticles in the canonical ensemble. The inorganic NBBs are modelled as spherical NPs, which interact with each other via a Hamaker potential.^{28,33} The PEO-based surfactant, F127, is represented by a bead-spring model with soft, non-bonded interactions,^{29,34} and the molecule is discretized into $N = 40$ coarse-grained beads with a structure of B₁₄A₁₂B₁₄. The end-to-end distance of F127 can be calculated as $R_{e0} \approx \sqrt{6}R_g = 8.475 \text{ nm}$, where $R_g = 3.46 \text{ nm}$ is the radius of gyration for F127, measured from SAXS experiments. This top-down model incorporates bonded interactions that describe the linear chain architecture and non-bonded interactions that give rise to microphase separation in the surfactant solution.²² Details of the calculation and potentials used are provided in the supporting information (SI).

Figures 5a and 5b show snapshots from the simulation system with the extreme values of $D_{\text{NBB}} = 2.54$ and 5.94 nm, respectively, after the system has reached a stationary state. While in the first case a very well-ordered mesostructure is observed, the system with larger NBB size shows significantly less-ordered mesostructures (see Figure S8, S9 and further discussion in SI). To evaluate the homogeneity of the mesostructure, the dispersity index (DI) was calculated for each simulation system (Figure 5c). DI is a criterion of a homogeneity of mesostructure in this study, a smaller DI signals implies a more homogenous mesostructure.

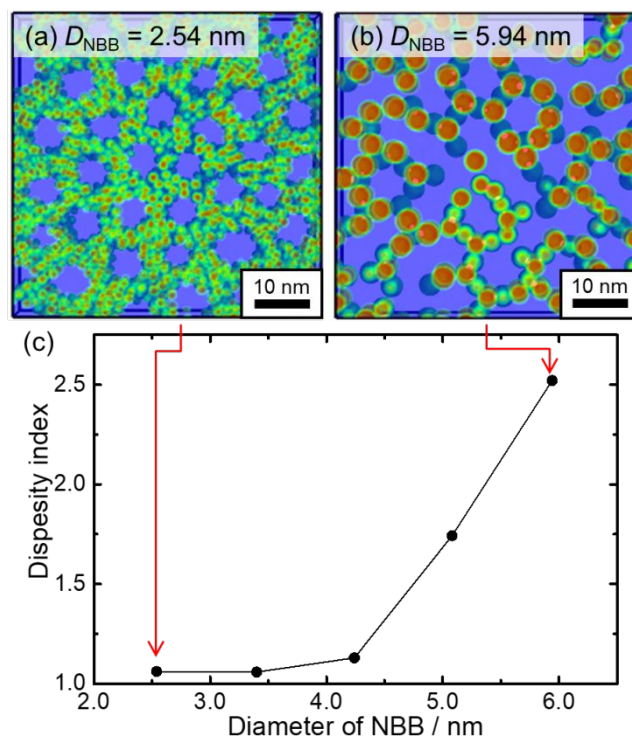


Figure 5. Typical snapshots of mesostructures formed with NBBs and F127 with $D_{\text{NBB}} =$ (a) 2.54 nm and (b) 5.94 nm. The system size of (a) is $61.02 \times 61.02 \times 7.63 \text{ nm}^3$ and of (b) is $68.65 \times 68.65 \times 7.63 \text{ nm}^3$. The red spheres, green rings and blue regions are the NBB core, the interface and the F127 filled parts, respectively. (c) The change of the DI calculated from snapshots along with the D_{NBB} .

While a relatively constant value of DI is observed for low NBB diameters, which is indicative of a well-defined mesostructure, a rapid increase of DI, indicating the less-ordered mesostructures, is observed once D_{NBB} is larger than 4.24 nm, which is around $0.25R_{e0}$. This critical value is consistent with the empirical estimation from experiments¹¹ and recent simulations³⁵ that the size of NBBs should be four times smaller than that of the micelles (the pore diameter is around $1.0R_{e0}$ in our simulation) to fit the curvature of the interface. Larger NBBs ($D_{\text{NBB}} > 0.25R_{e0}$) tend to strongly aggregate into large clusters that cannot well co-assemble with the surfactants, forming less-ordered mesostructures. Hillhouse et al. reported that silica mesostructures with decreasing curvature were formed with increasing aging time of the precursor solutions. This was attributed to an increase in the gyration radius of precursor silica polymer species along aging, that eventually led to unstable (less-ordered) structures for high condensation.^{20,21} This trend is in good agreement with our present study. Even if the condensation kinetics of silica and transition metals, is substantially different (in this case, controlled condensation leads to NBB of stable size), our model permits to rationalize the importance of the inorganic NBB size and interactions with the template in the formation kinetics of the mesostructures.

The appearance of the threshold value of D_{NBB} , above which DI drastically increases, mainly originates from the size (mis)match of NBBs and the surfactant morphology, and the contribution of the non-linear Hamaker potential (a stronger attractive interaction between larger inorganic NBBs), as well as the depletion interaction.²² The increase of D_{NBB} results in a rapid aggregation of NBBs, which collapses the ordered structure formed by the amphiphilic surfactants. This model is in excellent agreement with the observed experimental trends and illustrates not only the key role of D_{NBB} in flexible adaptation of NBBs to the micelle structure, but also, more importantly, the critical role of D_{NBB} in colloidal and depletion forces which put self-assembly process into the action. It is also worthy to emphasize that the designed coarse-grained simulations are not limited to the comparison with the low-valence metal hydroxides in current work, but also to mesoporous structures formed by other crystalline nanoparticles, such as titania³⁶, manganese oxide and ferrite nanocrystals,³⁷ which requires careful parameter mapping (see details in SI).

The effect of surface nature of NBB on the formation of mesoporous structures

As well as the value of D_{NBB} , the surface nature of NBBs influencing on the aggregative tendency upon drying in the EISA process is another important parameter. In a previous work on mesoporous titania, simulations permitted to explain the deleterious role of aggregation between the NBBs on the order of the mesoporous structures. Namely, strong NBB-NBB attraction results in aggregation, which in turn leads to a merging of the mesopores, thus leading to poorly defined mesostructures.²² In order to test the generality of this hypothesis, samples with higher aggregation tendency than the previously presented AA- $y-t$ were employed to investigate this point. When acetic acid was used (AcOH-2.0- t) instead of acrylic acid, the aggregation tendency was higher than that in the acrylic acid system (AA-2.0- t) (Figure S10). Residual Ni^{2+} ions, D_p , and zeta potentials of particles were comparable between both systems at a given reaction time (Table 1). However, the AcOH-containing colloids present a higher degree of aggregation, that results formation of a larger aggregate. This difference in the aggregation behavior suggests

a different interparticle interaction, originated from different depletion force and/or steric effect derived from both surface modifiers. This points out that attention has to be paid to the intimate structure and interactions in the NBB (i.e., using AA and AcOH as reaction controllers).

Figure 6 shows the SAXS patterns of films prepared from F-AcOH-2.0- t solutions. The resultant mesostructures were assigned to the same cubic mesostructures (space group; $Im\bar{3}m$) as F-AA- $y-t$ systems. However, the threshold of $D_{\text{NBB}} = 1.3$ nm for the formation of ordered mesostructures is significantly smaller compared with the F-AA- $y-t$ systems ($D_{\text{NBB}} < 7.5$ nm). It is interesting to remark that albeit the AcOH-derived NBB are small and in principle should lead to a high level of organization, they tend to aggregate (as discussed above), which results in an increase of the effective size of the building blocks and subsequently changes the effective interactions with the template. D_s of the F-AcOH-2.0 systems begins to increase significantly after 20 minutes aging with respect to the equivalent AA-derived samples. In the case of F-AcOH-2.0-60, for example, $D_s = 7.9$ nm, which is in fact practically twice the critical NBB size found in the theoretical model for obtaining ordered mesostructures. This demonstrates that the aggregation tendency is an essential parameter to synthesize highly organized mesostructures, which should be taken care of, as well as controlling the D_{NBB} below a certain critical size.

Table 1. The comparison of AA-2.0- t and AcOH-2.0- t systems.

ID	Residual Ni^{2+} (%)	D_p / nm	D_s / nm	Zeta potential / mV (pH)
AA-2.0-5	33.0	0.74	N/A	29.6 (8.0)
AA-2.0-60	4.4	2.1	N/A	32.2 (8.2)
AcOH-2.0-5	33.7	0.99	N/A	28.6 (6.2)
AcOH-2.0-60	3.9	2.0	7.9	32.9 (8.3)

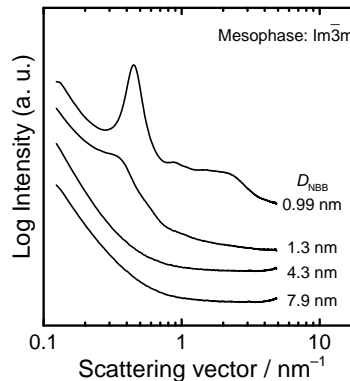


Figure 6. SAXS patterns of casted-films after drying at 120 °C for 2h. The casted-films composed of $D_{\text{NBB}} = 0.99$ nm, 1.3 nm, 4.3 nm, and 7.9 nm were prepared from F-AcOH-2.0-5, F-AcOH-2.0-10, F-AcOH-2.0-30, and F-AcOH-2.0-60, respectively. D_{NBB} of 4.3 nm and 7.9 nm are D_s and their D_p are 1.7 nm and 2.0 nm, respectively.

Extending the ANBB Approach to Other Transition Metal Hydroxides.

The ANBB approach presented above was extended to hydroxide NBBs for a series of divalent elements (Mn, Fe, Co, and Cu), based on the insights obtained in the α -Ni(OH)₂ NBB system. Since these divalent elements form metal hydroxides following dissimilar crystallization kinetics, acrylic acid used in the above discussion is only applicable to Ni, Co, and Fe systems. We found that the choice of carboxylic acids with different coordination strengths allows us to further optimize the crystallization kinetics and thereby extend ANBB approach to these systems. Relatively large crystals tend to form when glutaric acid or acrylic acid are used and prevents the formation of ordered mesostructures. Whereas, crystallite sizes can be small enough as NBBs (< 2 nm) when citric acid was employed, allowing to form ordered mesostructures (Figure S11 and Table S1). As a result, the use of citric acid with the highest coordination strength among the three carboxylic acids allows to proceed ANBB even for Cu and Mn systems. The strong complexation ability of citrate with several kinds of divalent metal ions in this study is in good agreement with reported study toward templated mesoporous oxide and carbonate materials.³⁸ Mesoporous structure can be obtained after subsequent heat-treatment at 250 °C (Figure 7). According to the literature,³⁹ metal hydroxo clusters can be formed through M-OH-M bond formation upon leaving of the aqua-ligand. Therefore, the rate of the formation of NBBs strongly depends on a lability of the ligand. A polyprotic carboxylic acid with stronger coordination characteristic can be used for a divalent metal element with more labile aqua-ligand. Through this route, a general and versatile synthesis of the metal hydroxo NBB and their assembly into mesostructured films can be achieved by simply optimizing the kinetics of crystal growth and aggregation. High ordering is allowed by the appropriate choice and combination of the metal ion and an adequate carboxylic acid.

In addition, layered hydroxide precursors present a second advantage: a variety of anions can be included in the interlayer. These chemical species can be used as ion sources for obtaining novel structures. Although we did not explore in-depth this feature in this work, our previous report demonstrated that substituted mesoporous Ni(OH)₂ hydroxides can be converted to oxide, sulfide, carbide, and carbon-composite by heat-treatment. These phases preserved well-defined mesostructure, due to the pseudomorphic transformation between the hydroxide and the final phase at moderate temperatures.¹⁹ A further study on the thermal behavior of the mesoporous metal hydroxides containing a series of divalent elements (Mn, Fe, Co, and Cu) is ongoing, and will also open up another class of chemical versatility in anionic species and/or valence state.

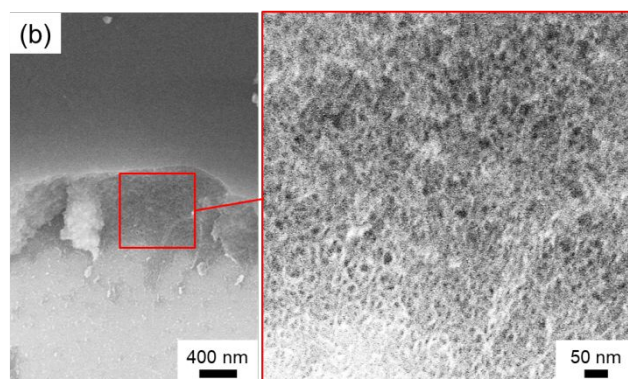
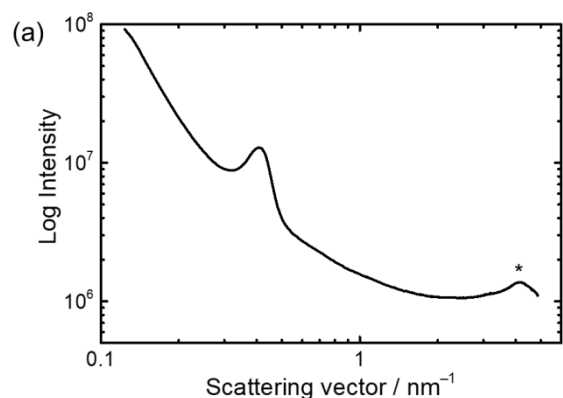


Figure 7. SAXS patterns of cast-film of Co-Cit-0.67-0.5 after drying at 120 °C for 2h. (b) Cross sectional SEM images of Co-Cit-0.67-0.5 after heat treatment at 120 °C for 2 h and 250 °C for 2 h. *: background peaks from α -Co(OH)₂ and/or polyimide

Conclusion

In this work, we report the controlled synthesis of colloidal α -Ni(OH)₂ NBBs with a variety of diameters in the nanometer scale -from oligomer to over 20 nm via a homogeneous epoxide-mediated alkalization process. Highly ordered mesostructures were obtained when the α -Ni(OH)₂ NBBs with a size less than a critical value were employed in combination with F127 templates. A computational model in conjunction with simulations showed an excellent agreement with experimental results and predictive power, which is useful for the actual design of the synthetic pathway. This analysis reveals that the D_{NBB} is a critical parameter to obtain the ordered mesoporous structures. It was also found that the surface nature (aggregation tendency of NBBs) significantly affects the thresholds of D_{NBB} toward ordered mesostructures; the NBBs with lower aggregation tendency showed a wider D_{NBB} range for ordered mesostructure formation. To prepare NBBs and mesostructured films for a variety of chemical compositions, an appropriate combination of a metal and a carboxylic acid in each system is mandatory for the inhibition of crystal growth and retarding aggregation. The approach demonstrated here is a promising general route to access versatile functional mesoporous and mesostructured materials, in particular those based on low-valence transition metal oxides. In addition, as this method is based on EISA, a flexible processing can lead towards thin films, xerogels or aerosols.

We anticipate that this pathway that employs pre-defined, controlled and stable inorganic NBBs will permit to circumvent the chemical complexities of solution processing. In addition, the feedback between experiments and theory permits

to consider a “chemistry of objects”, in which the co-self-assembly of pre-programmed soft and colloidal objects can be envisioned. Following a simple set of rules, based on controlling the size of different NBB, their interactions and aggregation behavior, complex architectures can be created by simple combination of building blocks “from the shelf”.

ASSOCIATED CONTENT

Supporting Information. FT-IR spectra, UV-Vis-NIR spectra, PXRD patterns, SAXS patterns, simulated snapshots, N₂ sorption/desorption, TEM image. This material is available free of charge via the Internet at <http://pubs.acs.org>.

AUTHOR INFORMATION

Corresponding Author

* E-mail (Y. Tokudome): tokudome@photomater.com

* E-mail (G. J. A. A. Soler-Illia): gsoler-illia@unsam.edu.ar

* E-mail (Q. Tang) qiyun.tang@theorie.physik.uni-goettingen.de

Present address of NT: Department of Chemical Science and Technology, Faculty of Bioscience and Applied Chemistry, Hosei University, Koganei, Tokyo 184-8584, Japan

ACKNOWLEDGMENT

Strategic Young Researcher Overseas Visits Program for Accelerating Brain Circulation from JSPS is gratefully acknowledged. The present work is partially supported by JSPS KAKENHI, JSPS bilateral program, LNLS proposal SAXS1 18927, ANPCyT (PICT 2014-3687 and 2015-3526), UBACyT (20020130100610BA), The Sumitomo Foundation, Izumi Science and Technology Foundation and Deutsche Forschungsgemeinschaft under grant Mu1674/15-1. The simulations have been performed at the GWDG Göttingen, the HLRN Hannover/Berlin, and the von-Neumann Institute for Computing, Jülich, Germany.

REFERENCES

- (1) Guo, J.; Tardy, B.; Christofferson, A.; Dai, Y.; Richardson, J.; Zhu, W.; Hu, M.; Ju, Y.; Cui, J.; Dagastine, R.; Yarovsky, I.; Caruso, F. Modular Assembly of Superstructures from Polyphenol-Functionalized Building Blocks. *Nat. Nanotechnol.* **2016**, *11*, 1105–1111.
- (2) Armao, J.; Nyrkova, I.; Fuks, G.; Osypenko, A.; Maaloum, M.; Moulin, E.; Arenal, R.; Gavati, O.; Semenov, A.; Giuseppone, N. Anisotropic Self-Assembly of Supramolecular Polymers and Plasmonic Nanoparticles at the Liquid-Liquid Interface. *J. Am. Chem. Soc.* **2017**, *139*, 2345–2350.
- (3) Wang, Y.; Price, A.; Caruso, F. Nanoporous Colloids: Building Blocks for a New Generation of Structured Materials. *J. Mater. Chem.* **2009**, *19*, 6451–6464.
- (4) Ding, H.; Liu, C.; Gu, H.; Zhao, Y.; Wang, B.; Gu, Z. Responsive Colloidal Crystal for Spectrometer Grating. *ACS Photonics* **2014**, *1*, 121–126.
- (5) Tokudome, Y.; Nakanishi, K.; Kanamori, K.; Fujita, K.; Akamatsu, H.; Hanada, T. Structural Characterization of Hierarchically Porous Alumina Aerogel and Xerogel Monoliths. *J. Colloid Interface Sci.* **2009**, *338*, 506–513.
- (6) Yamada, Y.; Tsung, C.-K.; Huang, W.; Huo, Z.; Habas, S.; Soejima, T.; Aliaga, C.; Somorjai, G.; Yang, P. Nanocrystal Bilayer for Tandem Catalysis. *Nat. Chem.* **2011**, *3*, 372–376.
- (7) Wang, Y.; Jenkins, I.; McGinley, J.; Sinno, T.; Crocker, J. Colloidal Crystals with Diamond Symmetry at Optical Lengthscales. *Nat. Commun.* **2017**, *8*, 14173.
- (8) Xiao, X.; Yu, H.; Jin, H.; Wu, M.; Fang, Y.; Sun, J.; Hu, Z.; Li, T.; Wu, J.; Huang, L.; Gogotsi, Y.; Zhou, J. Salt-Templated Synthesis of 2D Metallic MoN and Other Nitrides. *ACS Nano* **2017**, *11*, 2180–2186.
- (9) Li, B. W.; Osada, M.; Ozawa, T. C.; Ebina, Y.; Akatsuka, K.; Ma, R.; Funakubo, H.; Sasaki, T., Engineered Interfaces of Artificial Perovskite Oxide Superlattices via Nanosheet Deposition Process. *ACS Nano* **2010**, *4*, 6673–6680.
- (10) Wang, L.; Wang, D.; Dong, X. Y.; Zhang, Z. J.; Pei, X. F.; Chen, X. J.; Chena, B.; Jin, J. Layered assembly of graphene oxide and Co–Al layered double hydroxide nanosheets as electrode materials for supercapacitors. *Chem. Commun.* **2011**, *47*, 3556–3558.
- (11) Sanchez, C.; Boissière, C.; Grosso, D.; Laberty, C.; Nicole, L. Design, Synthesis, and Properties of Inorganic and Hybrid Thin Films Having Periodically Organized Nanoporosity. *Chem. Mater.* **2008**, *20*, 682–737.
- (12) Wong, M.; Jeng, E.; Ying, J. Supramolecular Templating of Thermally Stable Crystalline Mesoporous Metal Oxides Using Nanoparticulate Precursors. *Nano Lett.* **2001**, *1*, 637–642.
- (13) Hwang, Y.; Lee, K.-C.; Kwon, Y.-U. Nanoparticle Routes to Mesoporous Titania Thin Films. *Chem. Commun.* **2001**, 1738–1739.
- (14) Chane-Ching, J.; Cobo, F.; Aubert, D.; Harvey, H.; Airiau, M.; Corma, A. A General Method for the Synthesis of Nanostructured Large-Surface-Area Materials through the Self-Assembly of Functionalized Nanoparticles. *Chem. - Eur. J.* **2005**, *11*, 979–987.
- (15) Fan, K.; Chen, H.; Ji, Y.; Huang, H.; Claesson, P.; Daniel, Q.; Philippe, B.; Rensmo, H.; Li, F.; Luo, Y.; Sun, L. Nickel-Vanadium Monolayer Double Hydroxide for Efficient Electrochemical Water Oxidation. *Nat. Commun.* **2016**, *7*, 11981.
- (16) Nguyen, T.; Boudard, M.; Carmezim, J.; Montemor, F. Ni_xCo_{1-x}(OH)₂ Nanosheets on Carbon Nanofoam Paper as High Areal Capacity Electrodes for Hybrid Supercapacitors. *Energy* **2017**, *126*, 208–216.
- (17) Lee, A. F.; Bennett, J. A.; Manayil, J. C.; Wilson, K. Heterogeneous catalysis for sustainable biodiesel production via esterification and transesterification. *Chem. Soc. Rev.* **2014**, *43*, 7887–7916.
- (18) Yu, X.-Y.; Luo, T.; Jia, Y.; Xu, R.-X.; Gao, C.; Zhang, Y.-X.; Liu, J.-H.; Huang, X.-J. Three-Dimensional Hierarchical Flower-like Mg–Al-Layered Double Hydroxides: Highly Efficient Adsorbents for As(v) and Cr(vi) Removal. *Nanoscale* **2012**, *4*, 3466–3474.
- (19) Tarutani, N.; Tokudome, Y.; Jobbágy, M.; Viva, F.; Soler-Illia, G.; Takahashi, M. Single-Nanometer-Sized Low-Valence Metal Hydroxide Crystals: Synthesis via Epoxide-Mediated Alkalinization and Assembly toward Functional Mesoporous Materials. *Chem. Mater.* **2016**, *28*, 5606–5610.
- (20) Bollmann, L.; Urade, V. N.; Hillhouse, H. W. Controlling Interfacial Curvature in Nanoporous Silica Films Formed by Evaporation-Induced Self-Assembly from Nonionic Surfactants. I. Evolution of Nanoscale Structures in Coating Solutions. *Langmuir*, **2007**, *23*, 4257–4267.
- (21) Urade, V. N.; Bollmann, L.; Kowalski, J. D.; Tate, M. P.; Hillhouse, H. W. Controlling Interfacial Curvature in Nanoporous Silica Films Formed by Evaporation-Induced Self-Assembly from Nonionic Surfactants. II. Effect of Processing Parameters on Film Structure. *Langmuir*, **2007**, *23*, 4268–4278.
- (22) Tang, Q.; Angelomé, P. C.; Soler-Illia, G. J. A. A.; Müller, M. Formation of Ordered Mesostructured TiO₂ Thin Films: A Soft Coarse-Grained Simulation Study. *Phys. Chem. Chem. Phys.* **2017**, *19*, 28249–28262.
- (23) Gash, A.; Tillotson, T.; Satcher, J.; Poco, J.; Hrubesh, L.; Simpson, R. Use of Epoxides in the Sol–Gel Synthesis of Porous Iron(III) Oxide Monoliths from Fe(III) Salts. *Chem. Mater.* **2001**, *13*, 999–1007.
- (24) Tokudome, Y.; Tarutani, N.; Nakanishi, K.; Takahashi, M. Layered Double Hydroxide (LDH)-Based Monolith with Interconnected Hierarchical Channels: Enhanced Sorption Affinity for Anionic Species. *J. Mater. Chem. A* **2013**, *1*, 7702–7708.
- (25) Jobbágy, M.; Soler-Illia, G. J. A. A.; Regazzoni, A. E.; Blesa, M. A. Synthesis of Copper(II)-Containing Nickel(II) Hydroxide Particles as Precursors of Copper(II)-Substituted Nickel(II) Oxides. *Chem. Mater.* **1998**, *10*, 1632–1637.
- (26) Soler-Illia, G. J. A. A.; Jobbágy, M.; Regazzoni, A. E.; Blesa, M. A. Synthesis of Nickel Hydroxide by Homogeneous Alkalinization. Precipitation Mechanism. *Chem. Mater.* **1999**, *11*, 3140–3146.
- (27) Manceau, A.; Calas, G.; Decarreau, A. Nickel-Bearing Clay Minerals: I. Optical Spectroscopic Study of Nickel Crystal Chemistry. *Clay Miner.* **1985**, *20*, 367–387.
- (28) Poul, L.; Jouini, N.; Fiévet, F. Layered Hydroxide Metal Acetates (Metal = Zinc, Cobalt, and Nickel): Elaboration via

Hydrolysis in Polyol Medium and Comparative Study. *Chem. Mater.* **2000**, *12*, 3123-3132.

(29) Deacon, G.B.; Phillips R.J. Relationships Between the Carbon-Oxygen Stretching Frequencies of Carboxylate Complexes and the Type of Carboxylate Coordination. *Coord. Chem. Rev.* **1980**, *33*, 227-250.

(30) Soler-Illia, G. J. A. A.; Crepaldi, E. L.; Grosso, D.; Durand, D.; Sanchez, C. Structural Control in Self-Standing Mesoporous Silica Oriented Membranes and Xerogels. *Chem. Commun.*, **2002**, *0*, 2298-2299.

(31) Crepaldi, E. L.; Soler-Illia, G. J. A. A.; Grosso, D.; Cagnol, F.; Ribot, F.; Sanchez, C. Controlled Formation of Highly Organized Mesoporous Titania Thin Films: From Mesoporous Hybrids to Mesoporous Nanoanatase TiO₂. *J. Am. Chem. Soc.*, **2003**, *125*, 9770-9786.

(32) Lowell, S.; Shields, J. E.; Thomas, M. A.; Thommes, M. *Characterization of Porous Solids and Powders: Surface Area, Pore Size and Density*; Springer Science & Business Media: Berlin, Heidelberg, 2012; Chapter 4.

(33) Hamaker, H.C. The London—van der Waals Attraction Between Spherical Particles. *Physica* **1937**, *4*, 1058-1072.

(34) Müller, M. Studying Amphiphilic Self-assembly with Soft Coarse-Grained Models. *J. Stat. Phys.* **2011**, *145*, 967-1016.

(35) Xu, J.; Han, Y.; Cui, J.; Jiang, W. Size Selective Incorporation of Gold Nanoparticles in Diblock Copolymer Vesicle Wall. *Langmuir*, **2013**, *29*, 10383-10392.

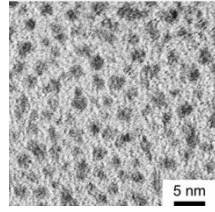
(36) Szeifert, J. M.; Feckl, J. M.; Fattakhova-Rohlfing, D.; Liu, Y.; Kalousek, V.; Rathousky, J.; Bein, T. Ultrasmall Titania Nanocrystals and Their Direct Assembly into Mesoporous Structures Showing Fast Lithium Insertion. *J. Am. Chem. Soc.*, **2010**, *132*, 12605-12611.

(37) Rauda, I. E.; Buonsanti, R.; Saldarriaga-Lopez, L. C.; Benjauthrit, K.; Schelhas, L. T.; Stefik, M.; Augustyn, V.; Ko, J.; Dunn, B.; Wiesner, U.; Milliron, D. J.; Tolbert, S. H. General Method for the Synthesis of Hierarchical Nanocrystal-Based Mesoporous Materials. *ACS Nano* **2012**, *6*, 6386-6399.

(38) Eckhardt, B.; Ortel, E.; Bernsmeier, D.; Polte, J.; Strasser, P.; Vainio, U.; Emmerling, F.; Kraehnert, R. Micelle-Templated Oxides and Carbonates of Zinc, Cobalt, and Aluminum and a Generalized Strategy for Their Synthesis. *Chem. Mater.* **2013**, *25*, 2749-2758.

(39) Livage, J.; Henry, M.; Sanchez, C. Sol-Gel Chemistry of Transition Metal Oxides. *Progress in Solid State Chemistry* **1988**, *18*, 259-341.

TOC Image



**LDH Nanobuilding
Blocks**



**Control of
Diameter and
Aggregation**

